EVALUATION OF FUTURE CLIMATE CHANGE SCENARIOS IN URBAN HEAT ISLAND AND ITS NEIGHBORHOOD USING DYNAMICAL DOWNSCALING

Marcos Vinícius Bueno de Morais[1,2*], Viviana Vanesa Urbina Guerrero[1],
Anderson Paulo Rudke[1], Thais Fujita[1], Leila Droprinchinski Martins[1,3],
Michelle Simões Reboita[4] and Jorge Alberto Martins[1,3]

[1]*Post-Graduation Program in Environmental Engineering, Federal Technological University, Londrina, Paraná, Brazil.*
[2]*Faculdade de Tecnologia, Garça, São Paulo, Brazil*
[3]*Visiting Researcher at Lund University, Lund, Sweden*
[4]*Universidade Federal de Itajubá, Itajubá, MG, Brazil*

Abstract: According to IPCC reports, global climate change is likely to be accompanied by a greater frequency, intensity, and duration of heat waves in urban areas. This is related to predicted and ongoing variation of atmospheric temperature and its association with the dynamical evolution of cities. Changes in the roughness pattern of the surface, wind intensity, soil available humidity and radiative properties compared to the natural surfaces characterize the formation of the Urban Heat Island (UHI). A dynamical downscaling of A2 and B1 SRES's future scenarios from Intergovernmental Panel on Climate Change were performed for Londrina, a medium-size city of Southern Brazil, using the Weather Research and Forecasting model. The main objective of this study is to investigate the impact of these scenarios on the UHI formation and intensity based on different input data, and its role and influence in the rural area. For this, an evaluation of the model and a comparison with the scenarios were done to mitigate the current trends. The results show a tendency in the current situation in following the pessimistic A2 scenario. Also, a drier rural area for the sustainable projection (B1) is found which implicates in a higher temperature and wind patterns modification for both sites, urban and rural region. Both future projections have a direct influence on the UHI intensity and formation, yielding effects in the agriculture and affecting conditions on human comfort over the region.

* Correspondence to: Marcos V. B. Morais, Tel.: +56 71 2 203 566
   E-mail: bmarcos@ucm.cl

INTRODUCTION

Urban areas are one of the most priority site in the study of the climate changes impacts over human health, since more than 50% of world population lives in urban regions (The World Bank, 2017). According to the last two IPCC reports (IPCC, 2007; Revi *et al.*, 2014), climate change is expected to lead increase in ill-health in many regions, especially in developing countries. For many kinds of disruption, heatwaves in urban areas will alter in frequency, intensity and duration in the furure (Ribeiro, 2008).

Previous studies have shown that urban areas are vulnerable to extreme events and climate changes (Nakicenovic *et al.*, 2000; Früh *et al.*, 2011; Hamdi *et al.*, 2015). For example, in 2003, around 35 thousand deaths were attributted to occurrence of a heat wave in the west Europe (Früh *et al.*, 2011), in 2010 in eastern Europe and Russia (Barriopedro *et al.*, 2011) and, in the summer of 2017, the Mediterran region endured heat wave 'Lucifer' (Guerreiro *et al.*, 2018). Numerical studies employing the A1B scenario from IPCC (Nakicenovic *et al.*, 2000) shows that the Frankfurt city, in Germany, could present more days (around 32 days) with maximum temperature above 25 ºC for the period between 2021 and 2050, when compared to 1971 to 2000 (Früh *et al.*, 2011). For Brussels and Paris, using the same A1B scenario, the projections show that the temperature will increase around 1.6 ºC and 1.8 ºC, respectively for 2050 (Hamdi *et al.*, 2015). This study also found a pattern in the changes of the temperatures between the city and rural areas. In this case, for the nocturnal period in the winter, the temperature has an increase of 0.2 ºC, while the diurnal in summer has a decrease in -0.1 ºC, which was resulted from a drier rural area.

The urban planning and its dynamics evolution can help to minimize the negative climate change effects. Stone *et al.* (2010) analyzed the association between urban form and the frequency of extreme heat events over a five-decade period for U.S. metropolitan regions. It was found that sprawling cities has two times more events by year when compared with compact regions. Simulation varying the growth of urban area in three different ways (current status, compact growth and spread growth) to the Metropolitan Area of Tokyo showed that the humid bulb temperature can increase in 4 ºC during the daytime, depending on the urban expansion mode in 2070 (Parker *et al.*, 2015). Similarly, using same city evolution scenarios for Paris in 2100, simulations also showed that the heat waves risk does not depends only of the densification dynamics, but also on exposure to heat of population, since higher densities may induce need for more cooling and increasing energy use (Lemonsu *et al.*, 2015). When the urban area is more compact, the population is more vulnerable to feel the effects of extreme temperatures, due its concentration is most impacted by heat island (Lemonsu *et al.*, 2015). The increase of temperature in the future can reduce the thermal comfort mainly in urban areas and enhance future burden of heat-related morbidity (Gronlund *et al.*, 2014). Some examples are excess hospital admissions by dehydration, heat stroke, and heat exhaustion, among people with underlying medical conditions (Semenza *et al.*, 1999; Watts *et al.*, 2017). Moreover, the interventions in the natural surface by the urbanization causes changes on roughness, reducing wind speed, moisture availability in the soil and radiative properties (Kalnay & Cai, 2003). These changes affect the local microclimate and can contribute to Urban Heat Island (UHI; Oke, 1988). This is a transient feature of urban areas, where the air temperature near the surface of the city is higher than the temperature of the surrounding rural areas, where buildings and streets release the heat absorbed during the day.

The study of UHI is very complex, owing the role of rural thermal input areas in generating the magnitude and the structure of UHI (Arnfield, 2003). Its intensity may vary due to the size of the city, wind speed, cloud cover (Montálvez *et al.*, 2000), and to the geographical location of the urban area, since differences between winter-summer or wet-dry contrast takes place (Arnfield, 2003). In mid-latitudes, the UHI is more intense during the night, while in tropical latitudes, its development takes place during the day (Oke, 1988; Montálvez *et al.*, 2000; Morris & Simmonds, 2000). Moreover, its intensity is strongly related to both morphology of cities and the construction material properties. The study of UHI is fundamental, because it can aggravate the effects of heat waves (Li & Bou-Zeid, 2013) and other extreme events. In addition, it affects the dispersion of pollutants due to local features and can become a public health problem (Dabbert *et al.*, 2000; Freitas, 2003; Ketzel *et al.*, 2002; Urbina Guerrero, 2010).

Several studies were addressed to assess changes in climate scenarios over Brazilian territory (Marengo & Ambrizzi, 2006; Marengo *et al.* 2009; Reboita *et al.*, 2014). However, considering Brazil's dimension, differences over climate conditions and its urban development, there is little practical use and more studies are needed to mitigate local effects and promote better understanding of the climate under high-resolution simulations. Considering the benefits of a good representation of atmospheric boundary conditions and more accurate forecast for urban regions, this work proposes the investigation of UHI formation and intensification in a medium sized-city located in a sub-

tropical region using numerical simulations as tool under future climate scenarios.

EXPERIMENTS

The study was conducted in the city of Londrina, in Brazil, which has approximately half a million inhabitants (IBGE, 2015), its geographical feature is shown in **Fig. 1**. Cities such as Londrina (100,000 to 500,000 inhabitants) represented about 27% of the Brazilian cities for the year 2010. Daytime UHI intensity in Londrina is about 2 ºC for a summer period (Capucim *et al*., 2014). The city has grown fast in terms of population and occupied area (Stamm *et al*., 2013; **Fig. 1**) and therefore, it is expected that the UHI intensity to increase.
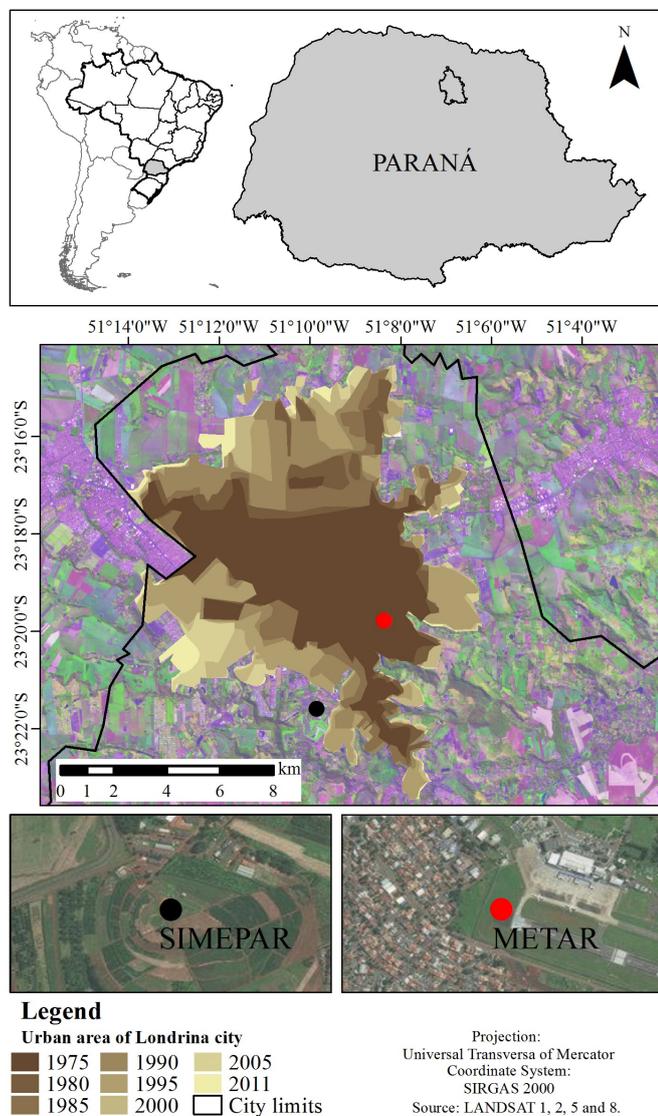
Fig. 1. Map of location of the study area. On the top map, the grid with more resolution. On the middle map, the urban area expansion during 1975 to 2011. Bottom map, are the meteorological station used for validation of the model.

Future Scenarios

The Special Report on Emission Scenarios (SRES) describes a series of future scenarios, developed by IPCC and characterize different directions for future developments. It also covers a wide range of characteristics such as demography, technology and economy that can influence pollutants emissions (Nakicenovic *et al.*, 2000). These scenarios use a variety of possibilities based on global development, which are associated to CO_2 sources and sinks, and other greenhouses gases, from alternative sources of energy to soil land use changes. The group of the qualitative storylines scenarios includes anthropogenic emissions from all of relevant greenhouse gas, besides other compounds, such as sulfur dioxide, carbon monoxide, nitrogen oxides and non-methane hydrocarbons. And given the uncertainties on future emissions and its increasingly irreversible directions, the exploit of these scenarios is an important task to enlighten the variability of the results in a changing climate.

In this work, it is considered the SRES scenarios A2 and B1 from IPCC, because they describe the pessimist and optimist scenarios, respectively. The A2 describes a very heterogeneous world, with continuous increasing of the population, and the per capita economic growth and technological change are more fragmented and slower than other storylines. On the other hand, the B1 storylines and scenario family describes a convergent world with the same global population, where the emphasis is on global solutions to economic, social and environmental sustainability, including improved equity, but without additional climate initiatives.

Numerical Modeling and Configuration

For this study, it was used the version 3.6.1 of the atmospheric model Weather Research and Forecast (WRF; Skamarock *et al.*, 2008). This model represents the last generation of numerical weather prediction, that works even for operational and research use. This model is in constant development, as a partnership of several agencies, like National Center for Atmospheric Research (NCAR), National Oceanic and Atmospheric Administration (NOAA), National Center for Environmental Prediction (NCEP), Forecast Systems Laboratory (FSL), Air Force Weather Agency (AFWA), and researcher and development agency around the world. The model can be executed even for ideal atmospheric situation as real situations, in a wide spectrum of horizontal scale application that vary from thousands of kilometers to few meters.

The meteorological outputs fields from Community Climate System Model, version 3 (CCSM 3; Collins *et al.*, 2006); for scenarios A2 and B1 (named here as SRESA2 and SRESB1) were used as initial and

boundary meteorological conditions for WRF to perform simulations. The CCSM3 system is composed of a group of coupled models capable of carrying out earth's climate system by simulating its atmosphere, ocean, land surface and sea-ice (Collins *et al.,* 2004; Oleson *et al*., 2004; Dickinson *et al.*, 2006; Briegleb *et al.*, 2004; Smith & Gent, 2002). To serve as atmospheric component of the CCSM3, the Community Atmosphere Model version 3 (CAM3) were applied and it is based on a spectral and Eulerian dynamic core with triangular spectral truncation at wave numbers 31, 42 and 85. The zonal grid spacing in the Equator ranges from 3.75º to 1.41º for the T31 and T85 configuration. The vertical dimension is treated using 26 levels with a hybrid coordinate that accompanies the terrain. In the model, this type of combination uses sigma coordinates at the lowest levels (which are influenced by topography), for the highest ones, only pressure levels is used, and at intermediate levels alternates between sigma coordinates and pressure. The surface model is integrated in the same horizontal grid as the atmospheric model, although each grid is divided to represent soil characteristics such as vegetation, urban areas, lakes and ice. Layers below the surface are used to represent the soil and sets a total of 10 (Mazzoli, 2003).

All global data from CCSM3, and the ones requested as input data to WRF, were adapted to a regular grid with horizontal homogeneous spacing of 1º and 30 isobaric vertical levels, and applied in the comparison with simulation resulted with the analysis of Global Forecasting System (GFS; Kanamitsu *et al.*, 1991). For this, it was selected a five days' term, from July 20th to 24th, 2015, a period with no rain and no clouds. The year 2015 was considered a prognostic period for future climate projections, since its historical simulations is between 1950 and 2005. All the results presented discard the first 24 h to prevent the spin-up effect (Daley, 1991).

The model was adjusted to have three nesting grids, with horizontal homogeneous spacing grid of 9, 3 and 1 km, centered in the city of Londrina (-23.3º, -51.1º; **Fig. 2**). In the vertical level, it was set 35 sigma levels, with the top in 50 hPa (about 20 km height). Table 1 shows the physical parameterizations used in the simulations with WRF model in this study. The land and soil use in all simulations are from Moderate-Resolution Imaging Spectroradiometer (MODIS), with horizontal spacing grid of 500 m (Schneider *et al.*, 2009).

Urban Canopy Model (UCM)

In order to better represent the physical processes involved in the exchange of momentum, heat and water vapor in urban environment in a mesoscale model, an UCM is coupled to the land surface model in WRF. The main purpose of this coupled model is to improve the description of lower boundary conditions and to provide more accurate forecasts for urban regions. The UCM (Kusaka & Kimura, 2004) is a single layer model, which has a simplified urban geometry. This scheme takes into account shadows from buildings, canyon orientation, diurnal variation of azimuth angle, multiple reflection of short- and long-wave radiation, the wind profile in the canopy layer, anthropogenic heating associated with energy consumption by human activities, and multilayer heat transfer equation for roof, wall and road surfaces. Considering the ability of the scheme to improve the calculations of surface energy budget in urban areas, coupled models have been widely used to investigate the effects and influences on the formation of urban heat islands (e.g. Tursilowati *et al.*, 2011; Morais *et al*., 2016; Lin *et al*., 2016).

Fig. 2. Nesting grid used in the simulations centered at Londrina. The red square represents the grid with 3 km of horizontal spacing grid, while the blue square is the high-resolution, with 1 km of horizontal spacing grid.

Table 1. Physical parameterization used for this study

Microphysics	Kessler Scheme (Kessler, 1969)
Cumulus	Grell-Freitas (Grell and Freitas, 2014)
Surface Layer	MM5 (Zhang and Anthes 1982)
Soil-Land Parameterization	Noah LSM (Chen and Dudhia, 2001)
Urban Parameterization	UCM (Kusaka and Kimura, 2004)
Boundary Layer	YUS (Hong et al. 2006)
Shortwave Radiation	Dudhia (Dudhia, 1989)
Longwave Radiation	RRTM (Mlawer et al, 1997)

RESULTS

To evaluate the model performance, statistical indexes were calculated using data from two observational surface stations located inside the Londrina (**Fig. 1**). The first one is from the Meteorological System of Paraná (SIMEPAR), located at 23.36º S and 51.1647º W, and the second is the METAR data from the airport located at 23.33º S, 51.14º W. The distance between stations is around of 4.6 km.

The normalized Taylor Diagram (Taylor, 2001) for temperature and specific humidity was used to analyzed the WRF outputs for both stations and for each different input data, where SRESA2 is the simulation with A2 scenario as input, SRESB1 is with B1 scenario and GFS is the simulation with GFS as input data. **Figures 3–4** show the comparison between the observations (named as reference) and the simulations results for temperature and specific humidity at 2 m, respectively.

Comparing the correlations of the model output for temperature with the observations (**Fig. 3**) for both datasets (SIMEPAR and METAR), a substantial higher correlation is notable for the GFS (r = 0.93 for METAR and 0.92 for SIMEPAR), while for the sustainable case (SRESB1) have the lowest values (r = 0.61 for METAR and r = 0.59 for SIMEPAR). For SRESA2 case, the correlation has higher values than the SRESB1, but not good as obtained for the GFS (r = 0.65 for METAR and 0.64 for SIMEPAR). The Root Mean Square (RMS) for GFS simulation is of 1.37 ºC, while for SRESB1 and SRESA2 are of 2.74 ºC and 3.62 ºC, respectively for METAR station. For SIMEPAR station, the RMS is also lower for GFS simulation compared with results from scenarios simulations (GFS – 1.46 ºC, SRESB1 – 2.92 ºC and SRESA2 - 3.66 ºC). The standard deviation for METAR data is of 3.18 ºC, while for GFS is of 3.40 ºC SRESB1 is 2.14 ºC and SRESA2 is 4.23 ºC for METAR. For SIMEPAR, the standard deviation values for observational data and simulation are similar those for METAR station. The result shows that GFS has a better skill, as expected since GFS is the simulation control, while the A2 scenarios has closer values to the GFS, indicating closeness between control and the pessimistic scenario.

For specific humidity, when comparing the correlations of the model output with the observations for both datasets (SIMEPAR and METAR), a better correlation is notable for the GFS (r = 0.85 for both METAR and SIMEPAR), while for the sustainable case (SRESB1) have the lowest values (r = 0.08 for METAR and r = 0.1 for SIMEPAR). For SRESA2 case, the correlation has higher values than the SRESB1, but not strong as GFS (r = 0.06 for METAR and 0.04 for SIMEPAR), when compared with observations records. The RMS for the GFS simulation is 0.70 g/kg, while
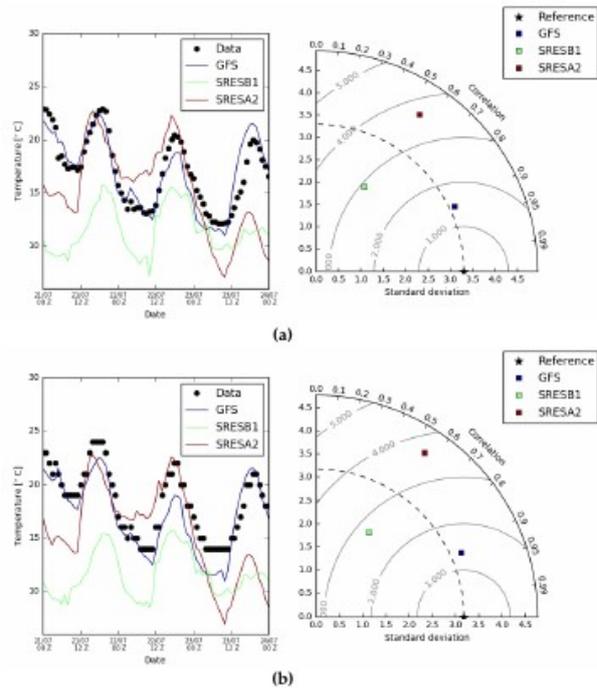
Fig. 3. Evolution of temperature (left column) and Taylor diagram (right collumn) for (a) SIMEPAR and (b) Londrina Airport METAR data stations. Blue line is the simulation with GFS as input and boundary conditions, green line is the simulation with B1 scenario and red line, is the simulation with A2 scenario. The last two are output from CCSM3 model.

SRESB1 and SRESA2 are 1.69 g/kg and 1.80 g/kg for METAR station. For SIMEPAR station, the RMS are close those obtained for other station. The standard deviation for METAR station are of 1.33 g/kg, 1.10 g/kg and 1.27 g/kg for GFS, SRESB1 and SRESA2, respectively, while the value obtained for observational data is 1.19 g/kg. For SIMEPAR station, the standard deviation for observational data is 1.14 g/kg, while for GFS simulation is 1.34 g/kg, SRESB1 is 1.08 g/kg and SRESA2, 1.22 g/kg. Like for temperature, the results show that GFS has a better skill to represent observation data, while the A2 scenario has closer values of the indexes to the GFS, comparing with the B1 scenario.

During the period of simulations, the highest intensity of UHI happens around 18 Z (15:00 Local Time) on July 22th. **Figure 5** presents the maps of temperature at 2 m for all simulations at this period. The difference of temperature at urban area and the rural adjacent area for GFS simulation is around 0.5 ºC (**Fig. 5c**), with a mean temperature for urban area of 18 ºC and 17.5 ºC for rural area. For SRESB1 simulation (**Fig. 5b**), temperature for both urban and rural area presents smaller magnitudes, with mean magnitudes of 16 ºC and 14 ºC, respectively. In this case, the UHI amplitude intensity grows to 2 ºC. In the SRESA2 simulation (**Fig. 5a**), the mean of the temperature difference is lower than that obtained with
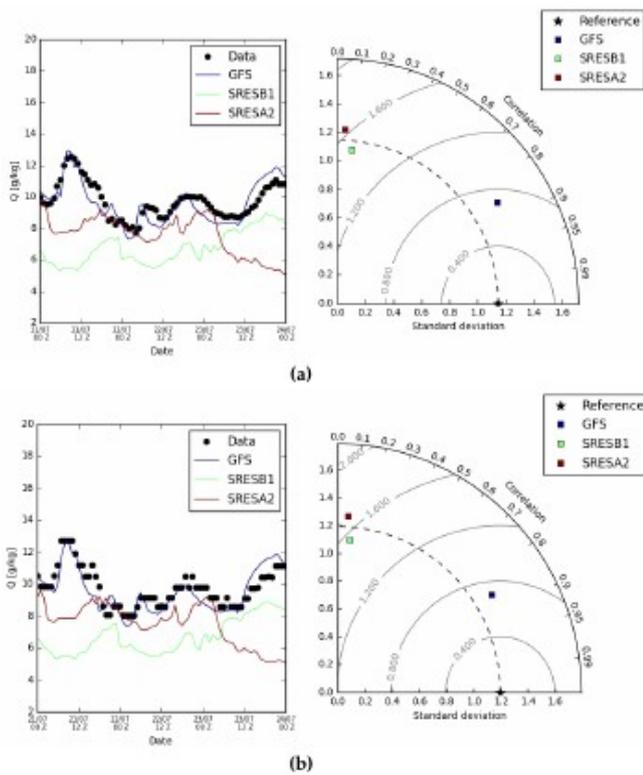
Fig. 4. Evolution of specific humidity (left column) and Taylor diagram (right collumn) for (a) SIMEPAR and (b) Londrina Airport METAR data stations. Blue line is the simulation control (with GFS as input and boundary conditions), green line is the simulation with B1 scenario and red line, is the simulation with A2 scenario. The last two are output from CCSM3 model.
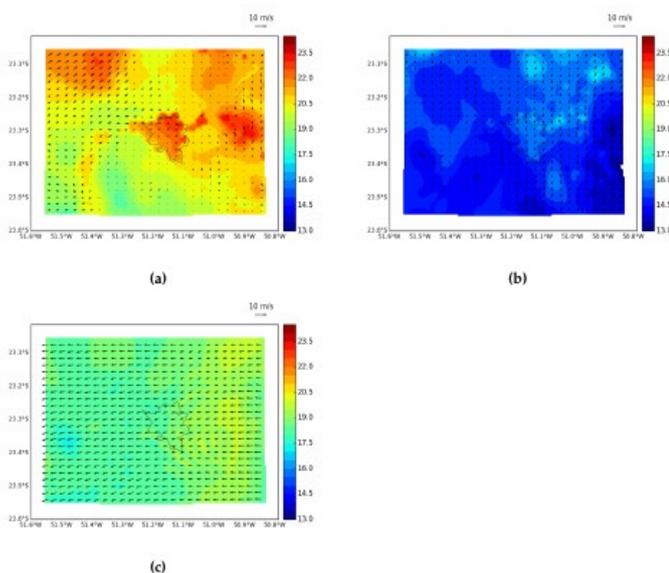
Fig. 5. Air temperature at 2 m (in ºC) at 18 on July 22th, 2015 for simulation with (a) SRESA2, (b) SRESB1 and (c) GFS simulation. Black arrow is the wind velocity intensity at 10 m.

SRESB1 simulation, reaching an amplitude intensity of 1 ºC. In spite of this, it is important to note that the increase in temperature occurs in both urban (22.5 ºC

average) and rural areas (21.5 ºC average), with similar values of peaks (23.5 ºC).

The pattern of the wind is also different among the simulations as can be observed in Figure 5. While an east wind is expected at this time of year (Figure 5c), in the case of the SRESB1 simulation a southern wind is noted. Meanwhile, in the SRESA2 simulation, besides the wind being of the west, a greater convergence happens in the incidence of urban region turning to south direction. It is also remarkable how much higher warming in the rural region influences the wind field in this simulation.

Fields of specific humidity at 2 m for all simulations at 18 Z on July 22th are shown in Figure 6. The SRESB1 simulation has drier values of humidity than SRESA2 and GFS in the urban area. At this time, the specific humidity is about 7.5 g/kg for SRESA2 simulation, while for GFS is about 9 g/kg. The SRESB1 simulation has lower values of specific humidity in the urban area, about 5.5 g/kg, it values are closer to the rural area (about 6.5 g/kg). The impact of climate scenarios is better visualized when the difference with the actual situation (considered the simulation with the GFS as input) is analyzed. **Figure 6** shows the result of these differences. The most pessimistic scenario (A2) presents a higher temperature difference in both rural and urban areas (**Fig. 6a**). In this case, the urban area is drier than the actual situation (**Fig. 6b**), while the rural area is more humid, with a difference of up to 3.5 g/kg of specific humidity. However, the more sustainable scenario (B1) has a lower temperature compared to the real situation (**Fig. 6c**), but both the urban and rural areas are drier than the GFS simulation (Figure 6d). This difference has influence in the lower intensity of UHI for B1 scenario.
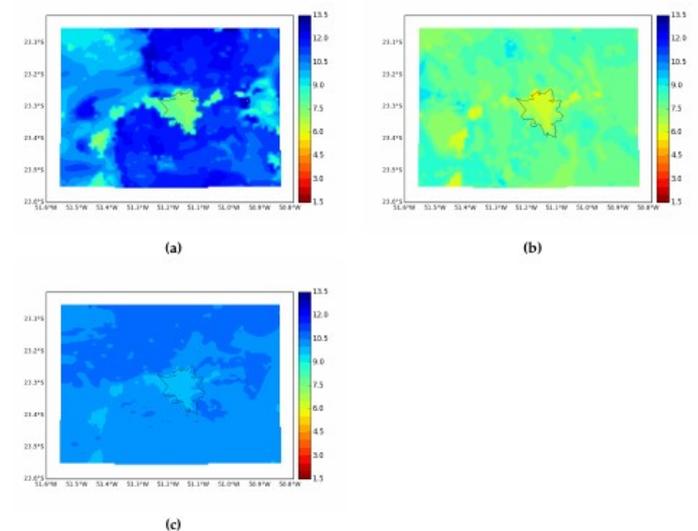
Fig. 6. Specific humidity at 2 m (in g/kg) at 18 Z on July 22th, 2015, for simulation with (a) SRESA2, (b) SRESB1 and (c) GFS simulation.
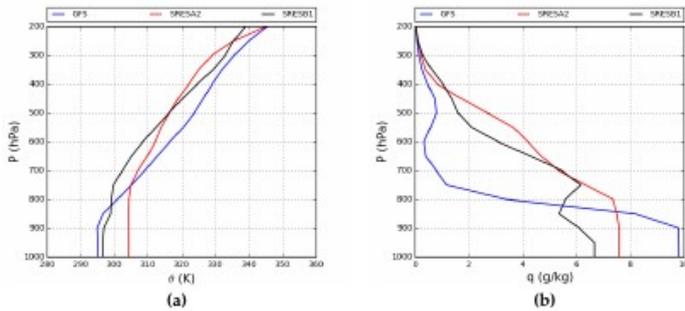
Fig. 7. Difference of air temperature at 2 m (in ºC) between (a) SRESA2 and GFS; (c) SRESB1 and GFS; and difference of specific humidity at 2 m (in g/kg) between (b) SRESA2 and GFS and (d) SRESB1 and GFS at 18 Z on July 22th, 2015.
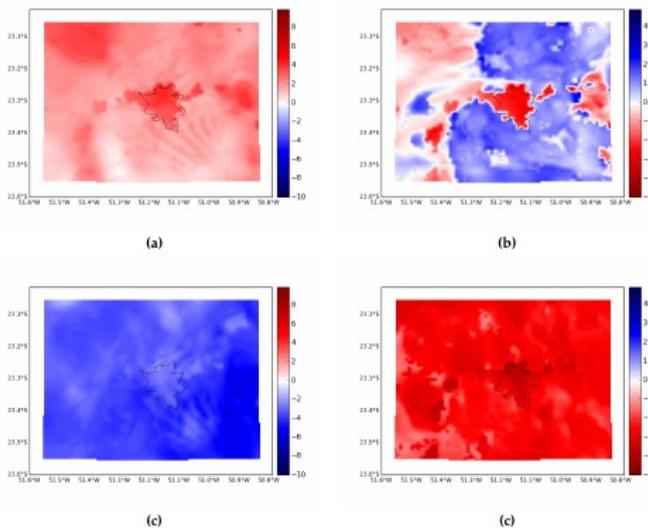
Fig. 8. Vertical profile of (a) potential temperature (in Kelvin) and (b) specific humidity (g/kg) in a point centered at urban area of Londrina (-23.3º, -51.1º).

Analyzing the vertical profiles of potential temperature and specific humidity at 18Z on July 22th, 2015, shown in Figure 8, the simulations with the scenarios A2 and B1 results in a warmer lower layers of atmosphere, with less content of water, when compared with the GFS model.

DISCUSSION AND CONCLUSION

This work presented an analysis of the physical processes in the formation and intensity of the UHI for the city of Londrina, using 3 dynamically downscaled scenarios: the present one—through the simulation with the GFS data as input; the SRESA2—using the A2 climate scenario, considered the most pessimistic; and SRESB1—using scenario B1, considered the most sustainable. The simulations were carried out for July, 2015, a five days' winter period, with no clouds or rain condition, considered a projection for the IPCC climate scenarios.

Considering the simulation of GFS, based on the evaluation of the model, it can be noted that the current situation for both temperature and specific humidity at 2 m, is more similar to presented by the A2 scenario than the B1. All SRESA2 indexes was closer to GFS than SRESB1. It can be seen in the peak of temperature on July 22th at 15 Z, when temperature values from SRESA2 are closer to than SRESB1 temperature values and RMS indexes regarding the period of the simulations.

It is remarkable how much the physical processes involved in the atmosphere influence the formation and intensity of the UHI. Even considering the more sustainable situation, the intensity of the realistic UHI was similar to the case of the most pessimistic situation. This is due to the fact that the rural region of the B1 case is drier than the A2 simulation. Thus, this has an influence on the energy budget at surface, confirming the high intensity of the UHI for B1 simulation. This is similar to that found in the literature, for example, by Hamdi *et al.* (2015), which the drier rural area found presented an important hole in the UHI development for Paris in the A1B scenario (considered balanced). In addition, B1 future scenario downscaled that presents a drier rural area, could be an implication in food production in this important agricultural area of Brazil.

The warmer lower layers of atmosphere with lower content of water found in the scenarios A2 and B1, when compared with the GFS model, implies that the vertical movement due UHI effects over the urban area is less probable to form convective nebulosity. On the other hand, in the medium and high layers of the atmosphere, the climatic scenarios present a greater probability of cloud formation with ice crystals, due to the higher content of humidity and lower temperature presented in these layers. This type of clouds affects the energy budget that arrives in the layers closer to the surface of the Earth, because they have more ice crystals that modifies the albedo and the radiative transfer (Lambert *et al.*, 2015).

The decrease on humidity affects directly the formation and the intensity of UHI. The higher value of the A2 scenarios affects the wind pattern at local scale, probably influencing on the pollutants dispersion. The greater convergence at urban area can configure a maintenance of high levels of poor air quality. Regarding human thermal comfort, dryer and warmer layers increase risks of heat-related illness or deaths, and for both A2 and B1 scenarios, it was found they get worse for future projection. Finally, the dynamical downscaling of future scenarios is an important tool to analyze its impact in a local scale.

REFERENCES

Arnfield, A.J. Two decades of Urban Climate Research: A review of Turbulence Exchanges of Energy and Water, and the Urban Heat Island. Int. J. Climatol. 2003, 23, 1–26.

Atkinson, B.W. Numerical Modelling of Urban Heat-Island Intensity. Bound. Layer Meteorol. 2003, 109, 285–310.

Barriopedro, D.; Fischer, E.M.; Luterbacher, J.; Trigo, R.M.; García-Herrera, R. The hot summer of 2010: redrawing the temperature record map of Europe. Science. 2011, 332(6026), 220-224.

Briegleb, B.P.; Bitz, C.M.; Hunke, E.C.; Lipscomb, W.H.; Holland, M. M.; Schramm, J.L.; Moritz, R.E. Scientific Description of the Sea Ice Component in the Community Climate System Model, Version Three; NCAR Technical Report; NCAR/TN-463STR; 2004. Boulder, Colorado, USA.

Capucim M.N.; Brand V.S.; Machado C.B.; Martins L.D.; Allasia D.G.; Homann C.T.; Freitas E.D.; Silva Dias, M.A.F.; Andrade, M.F.; Martins, J.A. South America land use and land cover assessment and preliminary analysis of their impacts on regional atmospheric modeling studies. IEEE J. Sel. Top .Appl. 2014, 8, 1185–1198.

Chen, F.; Dudhia, J. Coupling an advanced land surface-hydrology model with the Penn State-NCAR MM5 modeling system. Part I: Model implementation and sensitivity. Mon. Weather Rev. 2001, 129, 569–585.

Collins, W.D.; Bitz, C.M.; Blackmon, M.L.; Bonan, G.B.; Bretherton, C.S.; Carton, J.A.; Chang, P.; Doney, S. C.; Hack, J. J.; Henderson, T. B.; et al . The Community Climate System Model Version 3 (CCSM3). J. Clim. 2006, 19, 2122–2143.

Collins, W.D.; Rasch, P.J.; Boville, B.A.; J.; McCaa, J. R.; Williamson, D. L.; Kiehl, J. T.; Briegleb, B.; Bitz, C.; Lin, S. J.; et al . Description of the NCAR Community Atmosphere Model (CAM3); NCAR Technical Note; NCAR/TN-464+STR; 2004. Boulder, Colorado, USA.

Dabbert, W.F.; Hales, J.; Zubrick, S.; Crook, A.; Mueller, C.; Krajewski, W.; Doran, J. C.; Mueller, C.; King, C.; Keener, R. N.; et al Forecast Issues in the Urban Zone: Report of the 10th Prospectus Development Team of the U.S. Weather Research Program. Bull. Am. Meteorol. Soc. 2000, 81, 2047–2064.

Daley, R. Atmospheric Data Analysis; Cambridge Press: New York, NY, USA, 1991; pp. 1–457.

Dickinson, R.E.; Oleson, K.W.; Bonan, G.; Hoffman, F.; Thornton, P.; Vertenstein, M.; Yang, Z. L.; Zeng, X. The Community Land Model and its climate statistics as a component of the Community Climate System Model. J. Clim. 2006, 19, 2302–2324.

Dudhia, J. Numerical Study of Convection Observed during the Winter Monsoon Experiment Using a Mesoscale Two—Dimensional Model. J. Atmos. Sci. 1989, 46, 3077–3107.

Freitas, E.D. Circulações Locais em São Paulo e sua Influência na Dispersão de Poluentes. 157 f. Ph.D. Thesis, Atmospheric Science Department, University of São Paulo, São Paulo, Brazil, 2003.

Früh, B.; Becker, P.; Deutschlander, T.; Hessel, J.D.; Kossman, M.; Mieskes, I.; Namyslo, J.; Roos, M.; Sievers, U.; Steigerwald, T.; et al. Estimation of Climate-Change Impacts on the Urban Heat Load Using an Urban Climate Model and Regional Climate Projections. J. Appl. Meteorol. 2011, 50, 167–184.

Grell, G.A; Freitas, S.R. A scale and aerosol aware stochastic convective parameterization for weather and air quality modeling. Atmos. Chem. Phys. 2014, 14, 5233–5250.

Gronlund, C.J.; Zanobetti, A.; Schwartz, J.D.; Wellenius, G.A.; O'Neill, M.S. Heat, heat waves, and hospital admissions among the elderly in the United States, 1992–2006. Environ. health persp. 2014, 122(11), 1187.

Guerreiro, S.B.; Dawson, R.J.; Kilsby, C.; Lewis, E.; Ford, A. Future heat-waves, droughts and floods in 571 European cities. Environ. Res. Lett. 2018, 13(3), 034009.

Hamdi, R.; Giot, O.; De Troch, R.; Deckmyn, A.; Termonia, P. Future Climate of Brussels and Paris for the 2050s under A1B scenario. Urban Clim. 2015, 12, 160–182.

Hong, S.; Noh, Y.; Dudhia, J. A new vertical diffusion package with explicit treatment of entrainment processes. Mon. Weather Rev. 2006, 134, 2318–2341.

IBGE 2014: Data of South and Southeast Region of Brazil Avaiable online: http://www.ibge.gov.br/ (accessed on May 12th, 2017).

Intergovernmental Panel on Climate Change (IPCC). Climate Change 2007: The Physical Science Basis, Contribution of Working Group I. In: Fourth Assessment Report of the Intergovernmental Panel on Climate Change; Cambridge University Press: Cambridge, UK; New York, NY, USA, 2007; 996p.

Kalnay, E.; Cai, M. Impact of urbanization and land-use change on climate. Nature, 2003, 423, 528–531.

Kanamitsu, M.; Alpert, J.C., Campana, K.A; Caplan, P.M.; Deaven, D.G.; Iredell, M.; Katz, B.; Pan, H.L.; Sela, J.; White, G.H. Recent changes implemented into the global forecast system at NMC. Weather Forecast. 1991, 6, 425–436.

Kessler, E. On the Distribution and Continuity of Water Substance in Atmospheric Circulation; Meteorol. Monogr. 1969, 10, 88p.

Ketzel, M.; Berkowicz, R.; Muller, W.; Lohmeyer, A. Dependence of street canyon concentrations on above roof wind speed—Implications for numerical modelling. Int. J. Environ. Pollut. 2002, 17, 356–366.

Kusaka, H.; Kimura, F. Coupling a single-layer urban canopy model with a simple atmospheric model: Impact on urban heat island simulation for an idealized case. J. Meteorol. Soc. Jpn. 2004, 82, 67–80.

Lambert, F.H.; Webb, M.J.; Yoshimori, M.; Yokohata, T. The cloud radiative effect on the atmospheric energy budget and global mean precipitation. Clim. Dyn. 2015, 44, 7-8, 2301-2325.

Lemonsu, A.; Viguié, V.; Daniel, M.; Masson, V. Vulnerability to heat waves: Impact of urban expansion scenarios on urban heat island and heat stress in Paris (France). Urban Clim. 2015, 14, 586–605.

Li, D.; Bou-Zeid, E. Synergistic interactions between urban heat islands and heat waves: The impact in cities is larger than the sum of its parts. J. Appl. Meteorol. 2013, 52, 2051–2064.

Lin, C.-Y.; Su, C.J; Kusaka, H.; Akimoto, Y.; Sheng, Y.F.; Huang, J.C.; Hsu, H.H. Impact of an improved WRF urban canopy model on diurnal air temperature simulation over northern Taiwan. Atmos. Chem. Phys. 2016, 16, 1809-1822.

Marengo, J.A.; Ambrizzi, T. Use of regional climate models in impacts assessments and adaptations studies from continental to regional and local scales: The CREAS (Regional Climate Change Scenarios for South America) initiative in South America. In Proceedings of the 8th International Conference on Southern Hemisphere Meteorology and Oceanography (ICSHMO), Foz do Iguaçu, Brazil, 24–28 April 2006; pp. 291–296.

Marengo, J.A.; Jones, R.; Alves, L.M.; Valverde, M.C. Future change of temperature and precipitation extremes in South

America as derived from the PRECIS regional climate modeling system. Int. J. Climatol. 2009, 29, 2241–2255.

Mazzoli, C.R. Estudo Numérico da Influência das Mudanças Climáticas e das Emissões Urbanas no Ozônio Troposférico da Região Metropolitana de São Paulo. 162 f. Ph.D. Thesis, University of São Paulo, São Paulo, Brazil, 2003.

Mlawer, E.J.; Taubman, S.J.; Brown, P.D.; Iacono, M.J.; Clough, S.A Radiative transfer for inhomogeneous atmospheres: RRTM, a validated correlated-k model for the longwave. J. Geophys. Res. Atmos. 1997, 102, 16663–16682.

Montálvez, J.P.; Rodriguéz, A.; Jiménez, J.I. A study of the urban heat island of Granada. Int. J. Climatol. 2000, 20, 899–911.

Morais, M.V.B.; Freitas, E.D.; Urbina Guerrero, V.V.; Martins, L.D. A modeling analysis of urban canopy parameterization representing the vegetation effects in the megacity of São Paulo. Urb. Clim. 2016, 17, 102-115.

Morris, C.J.G.; Simmonds, I. Associations between varying magnitudes of the urban heat island and the synoptic climatology in Melbourne, Australia. Int. J. Climatol. 2000, 20, 1931–1954.

Nakicenovic, N.; Alcamo, J.; Davis, G.; Vries, B.; Fenhann, J.; Gaffin, S.; Kermeth G.; Amulf, G.; Jung, T. Y.; Kram, T. et al.. Special Report on Emission Scenarios, Published for the Intergovernamental Panel on Climate Change; Cambridge University Press,New York, NY, USA,: 2000; 608p.

Oke, T.R. Boundary Layer Climates, 2nd ed.; Cambridge University Press: New York, NY, USA, 1988; 435p.

Oleson, K.; Dai, Y.; Bonan, G.B.; Bosilovichm, M.; Dickinson, R.; Dirmeyer, P.; Hoffman, F.; Houser, P.; Levis, S.; Niu, G. Y.; et al. Technical Description of the Community Land Model (CLM); NCAR Technical Report; NCAR/TN-461+STR; 2004. Boulder, Colorado, USA.

Parker, A.S.; Kusaka, H.; Yamagata, Y. Assessment of the Impact of Metropolitan-Scale Urban Planning Scenarios on the Moist Thermal Environment under Global Warming: A Study of the Tokyo Metropolitan Area Using Regional Climate Modeling. Adv. Meteorol. 2015, 693754.

Reboita, M.S.; Rocha, R.P.; Dias, C.G.; Ynoue, R.Y. Climate Projections for South America: RegCM3 Driven by HadCM3 and ECHAM5. Adv. Meteorol. 2014, 376738.

Revi, A.; Satterthwaite, D.E.; Aragón-Durand, F.; Corfee-Morlot, J.; Kiunsi, R. B. R.; Pelling, M.; Roberts, D. C.; Solecki, W.; da Silva, J.; Dodman, D.; et al.. Urban areas. In: Climate Change 2014: Impacts, Adaptation, and Vulnerability. Part A: Global and Sectoral Aspects. Contribution of Working Group II to the Fifth Assessment Report of the Intergovernmental Panel on Climate Change; Field, C.B., Barros, V.R., Dokken, D.J., Mach, K.J., Mastrandrea, M.D., Bilir, T.E., Chatterjee, M., Ebi, K.L., Estrada, Y.O., Genova, R.C., et al., Eds.; Cambridge University Press: Cambridge, UK; New York, NY, USA, 2015; pp. 535–612.

Ribeiro, W.C. Impact of the climate changes in the cities of Brazil (Impacto das mudanças climáticas em cidades no Brasil). Parcer. Estratég. 2008, 27, 293–321. (In Portuguese).

Rosenzweig, C.; Solecki, W.; Hammer, S.A.; Mehrotra, S. Cities lead the way in climate-change action. Nature 2010, 467, 909–911.

Schneider, A.; Friedl, M.A.; Potere, D. A new map of global urban extent from MODIS data. Environ. Res. Lett. 2009, 4, 044003.

Semenza, J.C.; Mccullough, J.; Flanders, W.D.; Mcgeehin, M.A.; Rubin, C.H.; Lumpkin, J.R. Excess hospital admissions during the 1995 heat wave in Chicago. Am. J. Prev. Med. 1999, 16, 269–277.

Skamarock, W.C.; Klemp, J.B.; Dudhia, J.; Gill, D.O.; Barker, D.M.; Duda, M. G.; Huang, X. Y.; Wang, W.; Powers, J. G A Description of the Advanced Research WRF Version 3; NCAR Technical Note; NCAR/TN-475+STR; 2008. Boulder, Colorado, USA.

Smith, R.D.; Gent, P.R. Reference Manual for the Parallel Ocean Program (POP), Ocean Component of the Community Climate System Model (CCSM2.0 and 3.0); NCAR Technical Report; LA-UR-02-2484; 2002. Boulder, Colorado, USA.

Stone, B.; Hess, J.; Frumkin, H. Urban form and extreme heat events: are sprawling cities more vulnerable to climate change than compact cities? Environ Health Perspect. 2010, 118, 1425–1428.

Taylor, K.E. Summarizing multiple aspects of model performance in a single diagram. J. Geophys. Res. 2001, 106, 7183–7192.

Tursilowati, L.; Sumantyo, J.T.S.; Kuze, H.; Adiningsih, E.S. The integrated WRF/Urban modeling system and its application to monitoring urban heat island in Jakarta, Indonesia. J. Urban Environ. Engng. 2011, 6, 1 1-9. doi: 10.4090/juee.2012.v6n1.001009

Urbina Guerrero, V.V. Características das Circulações Locais em Regiões Metropolitanas do Chile Central. 113 f. Master's Thesis, Instituto de Astronomia, Geofísica e Ciências Atmosféricas, Universidade de São Paulo, São Paulo, Brazil, 2010.

Watts, N.; Amann, M.; Ayeb-Karlsson, S.; Belesova, K.; Bouley, T.; Boykoff, M.; Byass, P.; Cai, W.; Campbell-Lendrum, D.; Chambers, J.; et al. The Lancet Countdown on health and climate change: from 25 years of inaction to a global transformation for public health, In The Lancet, 2017.

Zhang, D.; Anthes, R.A. A High-Resolution Model of the Planetary Boundary Layer—Sensitivity Tests and Comparisons with SESAME-79 Data. J. App. Meteorol. 1982, 21, 1594–1609.